Impact Of Polyurethane Droplets on a Rigid Surface for Ink-Jet Printing

Wenchao Zhou, Drew Loney, Andrei G. Fedorov, F. Levent Degertekin, David W. Rosen
The George W. Woodruff School of Mechanical Engineering
Georgia Institute of Technology
813 Ferst Drive, Atlanta, GA, 30332-0405

Abstract

Ink-jet printing enables a more efficient, economic, scalable manufacturing process for a wider variety of materials than other traditional additive techniques. Understanding droplet impact onto a substrate is critical for accuracy control and optimization of the droplet deposition process. This paper reviews fundamentals of droplet impact behavior from literature, followed by our CFD simulations of droplet impact on a substrate. A numerical model is developed to simulate the transient flow dynamics during impact and spreading of an impinging droplet on a wetting rigid wall. The phase-field surface tracking technique is employed within a fixed (Eulerian) structured mesh. Simulation results are critically compared and validated with predictions of analytical models and experiments from literature. Droplet impact and spreading of a thermoplastic polyurethane material are investigated for SFF applications.

1. Introduction

Ink-jet printing manufacturing is an emerging technology which employs printing of a liquid-based precursor in an additive manufacturing process to create three-dimensional products. Streams of droplets, such as molten engineering materials, suspensions, or photopolymer liquids are ejected onto a solid substrate to build up intricate components by maneuvering both the print head and substrate. Although ink-jet printing manufacturing is conceptually an elegant technology, in practice it has not proven easy to implement because of a number of difficulties. These include control of the final shape of droplets, splash control, failure of droplets bonding to each other, formation of pores at the interface between droplets, and residual stress in the final part, among others. Achieving a good quality of the final parts requires accurate control of the whole deposition process, which demands a deep understanding of underlying physics for each deposition step.

Although the interaction of drops with surfaces has been extensively investigated for over a century, the development of comprehensive, predictive models has been difficult due to the complexity of the process and the interactions among many physical phenomena, including fluid mechanics, heat transfer, phase change, and surface chemistry. This paper first reviews previous research on this subject and identifies the key issues involved in understanding droplet impact behavior. Then, a numerical model is presented to help understand droplet impact using the phase-field surface tracking technique. Simulation results are critically compared with analytical models and experiments from the literature. Upon validation, the model is used to study the impact behavior of polyurethane droplet, a material of interest which has potential SFF applications.

2. Literature Review

To gain a better understanding of the droplet deposition process, previous research has been investigated, including droplet impact, droplet hardening and the coupling between them.

Droplet impact may result in various outcomes depending on the circumstances of impact. Upon impact on a solid surface, droplets can stick to the surface, bounce off the surface, spread on the surface or splash under different impact conditions [1]. Often the conditions leading to spreading and splashing are of particular interest. Due to the complexity of large deformation of the free surface and boundary conditions, different methods are employed to investigate this phenomenon, including experimental study, theoretical analysis and computer simulation.

When a droplet comes out of the ejector, it travels with the initial ejection velocity under the sum of gravity force, lift force and drag force caused by the surrounding atmosphere. Different models have been developed to approximate the impact velocity for the cases of high Reynolds number and low Reynolds number [2]. Droplet oscillations during flight were also modeled based on the droplet size [3].

When the droplet reaches the substrate, different observations have been made for different wettability cases between liquids and solids and the concept of contact angle was introduced to quantify this phenomenon. Contact angle hysteresis [4] is also observed when the droplet spreads out on the substrate, which refers to the difference between advancing contact angle and receding contact angle. It is believed that this difference is caused by surface inhomogeneity, surface roughness, impurities on the surface and temperature [5-6]. Due to the complexity of droplet impact behavior caused by the dynamic variation of the contact angle, experimental studies have been performed which suggest that the time evolution of the impact process can be divided into four distinct phases: the kinematic phase, the spreading phase, the relaxation phase and the wetting equilibrium phase [7]. These four impact regimes are classified according to the combination of driving forces and resisting forces to simplify the problem [8].

Increasing the impact velocity sufficiently will lead to a splash [9], which is undesirable for SFF. Three different kinds of splash have been identified according to their reasons, which are surrounding gas [10], surface roughness [11] and compliance of the solid substrate [12]. The splash caused by surrounding gas is referred as corona splash, while the splash caused by surface roughness and solid substrate compliance is referred as prompt splash. Previous experiments have shown that the splashing threshold follows the empirical relation $WeRe^{1/2}=K$, where K is a constant that depends on external parameters, such as surrounding gas pressure, surface roughness, etc. (Here, *We* refers to Weber number and *Re* refers to Reynolds number).

Theoretical analysis has been performed to help understand the impact process, including dimensionless parameters that allow generalization and construction of regime maps. An energy conservation analysis can be used to obtain a good solution of the final spreading radius of the droplet after impact with Reynolds number between 150 and 2000. Scale analysis can be used to get an estimation of the spreading velocity and time scales of driving and resisting forces under specific impact conditions [13]. To completely describe the whole impact process, 3-D differential equations are required to be built based upon a complete physical analysis, which is, however, far from being achieved. Therefore, mostly simplified 1-D models have been applied by only considering one parameter (the wetted area or the height of the droplet) to analyze the impact dynamics. Several 1-D models have been reviewed along with the dynamic contact angle models they used [14].

Numerical modeling has been also performed for the prediction of droplet impact behavior. Various numerical methods have been investigated, including Marker-and-Cell (MAC), Volume-

Of-Fluid (VOF), Level-Set, Phase-Field, and moving grids methods to predict droplet interface evolution upon transport towards and interaction with the substrate [15-19].

To build a 3-D structure, droplets must solidify after impact in a predictable manner. Three different approaches to solidification have been investigated in this field: droplets freezing, solvent evaporation (e.g., water) if a suspension solution is used, and photopolymer curing upon exposure to light or radiation. In the case of droplet freezing, several theoretical models for solidification of droplets have been reviewed, which suggest that the assumption that the droplet spreads first and then cools and solidifies is only valid within a limited parametric domain [15]. Most of the time, the spreading and solidification phenomena occur concurrently and are intimately coupled. Experimental studies on solidification, most of which use metal or hydrocarbon droplets of (1-4) mm in diameter with velocity of (1-3) m/s for easy observation [20], have also been undertaken and compared to numerical modeling, including development of different methods for treating the latent heat associated with phase change.

Drying the droplets containing suspended or dissolved solids is another way to obtain solids [21]. Solvent evaporation regimes have been identified, and different models have been developed with different assumptions [22]. Complimentary experimental studies were performed, as well [23-24]. Curing of photopolymer is another way to make a liquid droplet become solid [25]. Several mature industry applications of this method have been developed, including rapid prototyping machines from 3D Systems and Objet Technologies [26].

3. Numerical modeling

Since droplet impact could be very complicated in the most general case, several assumptions are made to simplify the analysis for the impact conditions of interest.

a) Since the impact velocities of interest are around 10m/s, which is much less than the speed of sound speeding the fluid, the fluid is assumed to be incompressible.
b) The shape of the droplet may oscillate from prolate to oblate during fall because of the effect of the surrounding atmosphere, which is negligible for droplet diameters less than about 3 mm [27]. Since we are concerned with much smaller (10s of micrometer in diameter) droplets, it is assumed to be spherical throughout the transit period and at impact.
c) The fluid flow is assumed to be Newtonian, and both liquid and gas flow are treated as laminar based on magnitude of the Reynolds number. The viscosity and surface tension are assumed to be constant during the impact.
d) The droplet and substrate are assumed to be isothermal.

With the assumptions above, the equations of conservation of momentum and mass can be formulated as follows:

$$\rho \frac{\partial \mathbf{u}}{\partial t} - \nabla \cdot [-p\mathbf{I} + \eta(\nabla \mathbf{u} + (\nabla \mathbf{u})^T)] + \rho \mathbf{u} \cdot \nabla \mathbf{u} = \mathbf{F} \quad (1)$$

$$\nabla \cdot \mathbf{u} = 0 \quad (2)$$

where: ρ is the fluid's density (kg/m^3); $\mathbf{u}$ is the velocity vector (m/s); p represents the pressure (Pa); η denotes the dynamic viscosity (Pa·s); $\mathbf{F}$ is the body force and $\mathbf{I}$ is the identity matrix.

Instead of directly tracking the interface between the liquid and gas, as well as the interface between liquid and solid using a moving (Lagrangian) grid, an Eulerian approach is used to locate the position of the interfaces on a fixed grid using the Phase-Field method.

3.1. Phase-Field Method

Different techniques exist for tracking an interface evolution numerically. The level-set method simply convects the interface with flow field, whereas the volume-of-fluid (VOF) method ensures volume conservation while convecting the interface. In this paper, the interfaces are tracked by the Phase-Field method, which not only convects the fluid interface but also ensures that the total energy of the system diminishes correctly. as described in [19]. A brief description of this method is given below.

In the Phase-Field method, the interface is diffuse and is defined by a dimensionless parameter ϕ that varies from -1 to 1. The volume fraction of each components of the binary fluid are $(1- \phi)/2$ and $(1+ \phi)/2$, for example, the first component is the air and the second component is the droplet for droplet deposition simulations. The volume fraction ϕ is advected by the fluid flow according to the following equations:

$$\frac{\partial \phi}{\partial t} + \mathbf{u} \cdot \nabla \phi = \nabla \cdot \frac{\gamma \lambda}{\varepsilon^2} \nabla \psi \tag{3}$$

$$\psi = -\nabla \cdot \varepsilon^2 \nabla \phi + (\phi^2 - 1)\phi \tag{4}$$

where γ is the mobility ($m^3 \cdot s/kg$), λ is the mixing energy density (N) and ε (m) is the interface thickness parameter. The mixing energy density and the interface thickness are related to the surface tension coefficient through:

$$\sigma = \frac{2\sqrt{2}\lambda}{3\varepsilon} \tag{5}$$

The volume fraction of the droplet is computed as,

$$V_f = \min(\max([(1 + \phi)/2],0),1) \tag{6}$$

And the density and dynamic viscosity are calculated by

$$\rho = \rho_1 + (\rho_2 - \rho_1)V_f \tag{7}$$

$$\phi = \phi_1 + (\phi_2 - \phi_1)V_f \tag{8}$$

where ρ_1 and ρ_2 are the densities and η_1 and η_2 are the dynamic viscosities of the air and the droplet, respectively.

The body force **F** in Equation (1) is broken down to four parts: gravity $\mathbf{F}_g$, surface tension $\mathbf{F}_{st}$, a force due to an external contribution to the free energy $\mathbf{F}_{ext}$ and a user defined body force $\mathbf{F}_u$ (e.g., electromagnetic or buoyancy forces if present).

$$\mathbf{F}_g = \rho \mathbf{g}; \qquad \mathbf{F}_{st} = G\nabla\phi; \qquad \mathbf{F}_{ext} = \left(\frac{\partial f_{ext}}{\partial \phi}\right)\nabla\phi \tag{9}$$

where **g** is gravity vector and G is the chemical potential (J/m^3),

$$G = \frac{\lambda\psi}{\varepsilon^2} \tag{10}$$

3.2. Numerical model

The numerical model is implemented using the commercially available software COMSOL 3.5a. A typical case is shown here to illustrate the implementation of the numerical model. Due to problem symmetry, the droplet and substrate can be modeled as shown in Figure 1, where the droplet comes out of the ejector at a certain distance from the substrate with an initial velocity. The droplet travels downward due to inertia and the gravity force and impinges on the rigid wall and spreads.

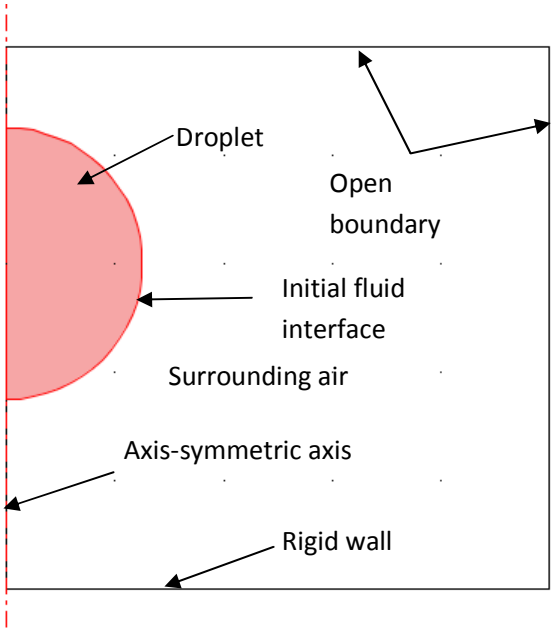

Figure 1 Geometry and boundary condition

The initial configuration is shown in Figure 1 and the diameter and initial velocity of droplet are 50 μm and 10m/s (downward), respectively. The boundary conditions are also shown in Figure 1 and the equilibrium contact angle between the droplet and the substrate is set to π/2. Table 1 gives the properties of droplet fluid and air used in the model simulations.

Table 1 Properties of materials

Medium	Density	Dynamic Viscosity	Surface Tension
Droplet	1,000 kg/m^3	0.01 Pa·s	0.07 N/m
Air	1.225 kg/m^3	1.789e-5 Pa·s	

Since the phase field method is not intrinsically mass conserving, the ideal situation would be of no artificial mass loss during the simulation, which would indicate high accuracy of simulations. Figure 2 shows the evolution of the droplet mass as function of time, as it moves from its initial

position towards the substrate. The maximum mass loss of the droplet during the entire simulated period is around 3%, and it can be reduced by further refining the mesh.

The form of the droplet during impact is often topologically-complex, but for SFF application the key factor is the spreading radius, which defines the resolution of this fabrication technique. Spreading radius is defined as the radius of the wetted area of the substrate. The change of spreading radius with time is shown in Figure 3, where we can see the spreading (up to about 15 micro seconds) and receding (beyond 15 micro seconds) of the droplet until it eventually reaches its equilibrium shape at about 150 micro second into the process.

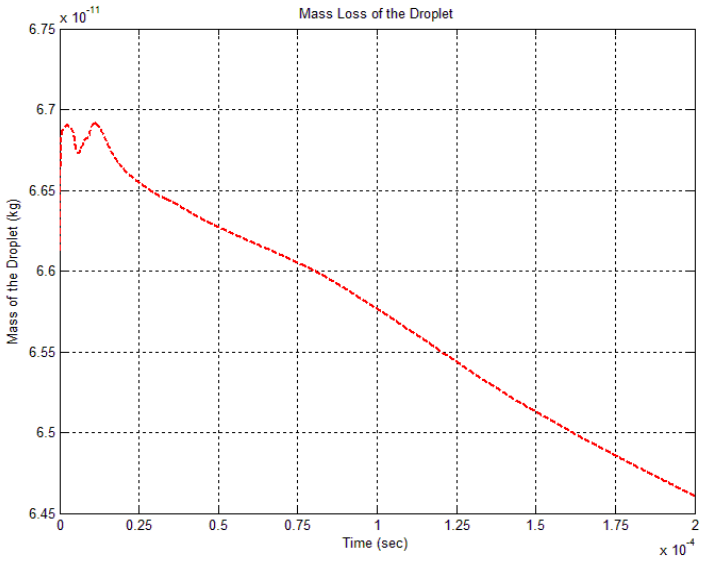

Figure 2 Mass change of the droplet due to numerical approximation of the interface

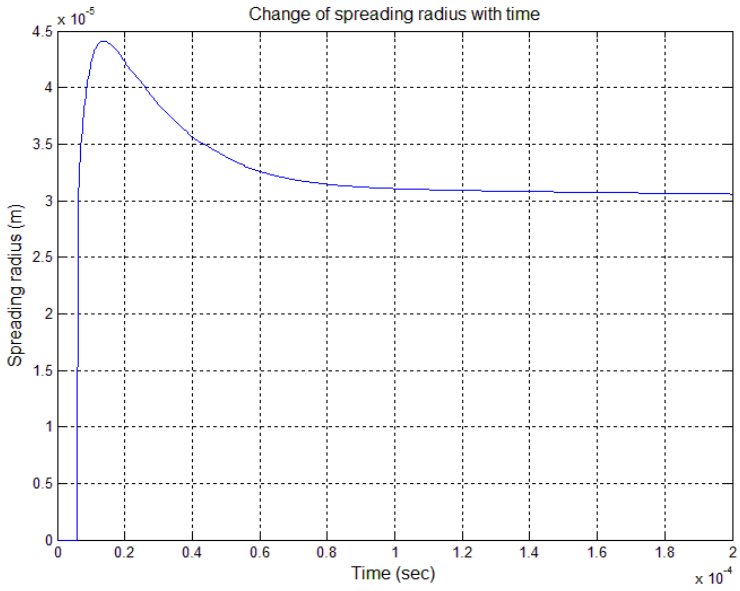

Figure 3 Change of spreading radius with time during the droplet impact

4. Validation

In order to validate the numerical model developed, a study of grid independence is conducted first, which includes assessment of the influence of the simulation domain extent and the mesh size refinement. The results of several static and dynamic analytical models are compared with those of the simulations. Finally, the simulation results are compared to the experimental results from literature for the impact condition of interest to SFF.

4.1. Grid & domain independence

The 'Open Boundary' condition is used in CAMSOL to simulate an infinite domain, and we examined if this boundary condition has any effects on the simulation results with different simulation domain sizes. To this end, the boundary length (the length of the boundary marked as 'open boundary' as Figure 1) was varied from 100μm to 300μm, and the simulation results showed a negligibly small change upon this variation. Therefore, the boundary length of 100 μm is sufficient to obtain accurate results for fluid flow simulations.

The grid independence validation ensures that the simulation results do not change significantly with different mesh sizes. In our numerical experiments, the minimum grid size of the mesh was changed from 4μm to 2μm and the results show that the mesh size of 4μm can provide sufficient accuracy in predicting the spreading radius and mass conservation.

4.2. Analytical validation

4.2.1. Equilibrium spread factor

The spread factor is defined as the ratio of spreading radius to the initial radius of the droplet, and the equilibrium spread factor is the spread factor when the droplet stops spreading, which is very important to determine the final shape of the droplet. Two analytical models for the equilibrium spread factor are compared with our simulation results. The first model is the spherical model, which assumes that the droplet during spreading maintains a sphere cap shape [28].

$$\beta_{equil} = 2[\frac{sin^3\theta_e}{(4 - 6cos\theta_e + 2cos^3\theta)}]^{1/3} \quad (11)$$

The simulation gives the equilibrium spread factor of β_{se}=1.2160, while the analytical result is β_{equil}=1.2599, yielding the relative error $|\beta_{equil} - \beta_{se}|/\beta_{se}$=3.61%. The second analytical model is cylindrical model, which assumes the droplet spreads as a self-similar cylinder [28].

$$\beta_{equil} = 2[\frac{1}{(6(1 - cos\theta_e)}]^{1/3} \quad (12)$$

The equilibrium spread factor for this model is β_{equil}=1.1006, and the relative error as compared to simulations is s $|\beta_{equil} - \beta_{se}|/ \beta_{se}$=.9.49%.

It can be seen that the simulation result is between that of the spherical and cylindrical models, where two extreme approximations are taken. The droplet shape under these impact conditions is neither a sphere cap nor a cylinder, but is more close to a sphere, which agrees well with results in the literature. Specifically, results demonstrate that, for viscous fluids impacting at low velocity, droplet shapes are close to spherical for the entire deposition process, while droplets of

low viscosity fluids have a spherical shape after reaching equilibrium, but not during dynamic spreading [28].

4.2.2. Maximum spread factor

Maximum spread factor is defined as the ratio of the maximum spread radius of the droplet to its initial radius. The maximum spread factor dictates how the spacing between nozzles in the array needs to be arranged and how the neighbor droplets interact with each other. There are many empirical [29-30] or semi-empirical [31-32] models to predict the maximum spread factor and the following empirical equation was shown to provide better predictions than other models [33]:

$$\left[0.2Oh^{0.33}We^{0.665}+\frac{1}{4}(1-cos\theta_e)\right]\beta_{max}^2+\frac{2}{3}\beta_{max}^{-1}=\frac{We}{12}+1 \tag{13}$$

where Oh is the Ohnesorge number, We is the Weber number, β_{max} is the maximum spread factor, and θ_e is the equilibrium contact angle.

Two simulations were run under different impact conditions and compared with the analytical model (Eq. 13), as shown in Table 2. It can be seen the simulation results agree well with the analytical results.

Table 2 Comparison of maximum spread factor between simulations and analytical model

	Droplet Radius	Impact Velocity	Dynamic Viscosity	Surface Tension	Droplet Density	Simulation Results	Theoretical Results	Relative Error
Case1	25μm	10m/s	0.01Pa·s	0.07N/m	1e3kg/m^3	1.7632	1.7476	0.88%
Case2	30μm	15m/s	8.94e-4Pa·s	0.072N/m	1e3kg/m^3	3.0667	3	2.71%

4.2.3. Dynamic spreading

In this section, the results of three well known 1D models for dynamic evolution of the wetted area/height of the droplet are compared with those of our numerical model under certain impact condition. The main challenge of the 1D model lies in the assumed physics of viscous dissipation and in the lack of self-consistency between the description of kinetic energy and that of dissipation. Bechtel et al. [34] first proposed a 1D model that is referred as the BBT model to include the change in kinetic energy using a variational method:

$$\begin{aligned}&\frac{1}{12}\frac{d}{dt}\left[\left(\frac{1+2h^3}{2h+h^4}\right)^2\left(\frac{1}{9}h^{-1}+\frac{11}{18}h^2+\frac{26}{45}h^5\right)\left(\frac{dh}{dt}\right)^2\right]\\&\qquad+\frac{d}{dt}\left[\frac{1}{3}[h^{-1}+2h^2-(h^{-1}-h^2)cos\theta_e]\right]\\&\qquad+\frac{\gamma}{18}Oh\frac{(h^3-1)^2(1+2h^3)^2}{h^4(2+h^3)^2}\left(\frac{dh}{dt}\right)^2=0\end{aligned} \tag{14}$$

With the initial conditions: $h|_{t=0}=1;\ \frac{dh}{dt}|_{t=0}=-\sqrt{We}$

where $h=\frac{H}{D_0};r=\frac{R}{D_0};\ r^2=\frac{1}{3}(h^{-1}-h^2);\ \gamma=\sqrt{\pi}Oh^{-1/2}$ and the coefficient $\sqrt{\pi}$ in the parameter γ is adjustable to the boundary layer thickness [31-35]; H and R are the droplet height

and the droplet radius during spreading, respectively; and D_0 is the initial droplet diameter. The comparison of results between the simulation and BBT model is shown in Figure 4, from which we can see that the results agree very well when the coefficient-multiplier of γ goes to 40. It is noteworthy that there is no rigorous calculation of γ and only a rough estimation can be made here.

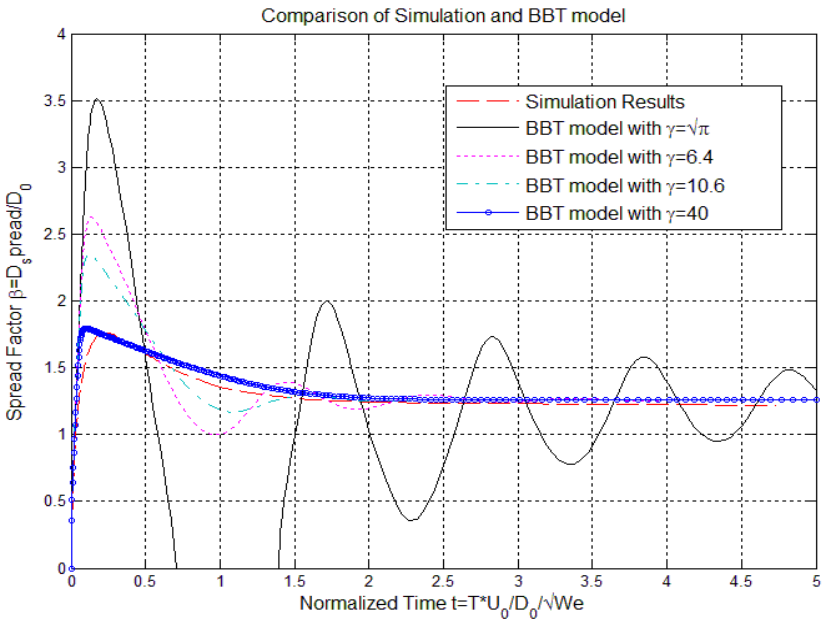

Figure 4 Comparison between simulation and BBT model

After that, various 1D models have been proposed [14, 29-33, 35]. Since the free surface of low viscosity droplets at its first maximum spreading is far from being spherical, the cylinder form was adopted by Kim et al. [35], which is called the KC model:

$$\frac{1}{12}\frac{d}{dt}\left[\left(\frac{1}{2}+\frac{1}{27}\frac{1}{r^6}\right)\left(\frac{dr}{dt}\right)^2\right]+\frac{d}{dt}\left[r^2(1-cos\theta_e)+\frac{1}{3r}\right]+\frac{\gamma}{2}Oh\,r^2\left(\frac{dr}{dt}\right)^2=0 \qquad (15)$$

with the initial conditions: $r_0^2(1-cos\theta_e)+\frac{1}{3r_0}=1;\ \frac{dr}{dt}|_{t=0}=\sqrt{We}\left(\frac{1}{2}+\frac{1}{27}\frac{1}{r^6}\right)^{-1/2}$

where $r=\frac{R}{D_0};\ \gamma=\sqrt{\pi}Oh^{-1/2}$ and the coefficient $\sqrt{\pi}$ in the parameter γ is adjustable. The results are compared with simulation results as shown in Figure 5. When the coefficient-multiplier of γ goes to 20, the KC model corresponds with the simulation results.

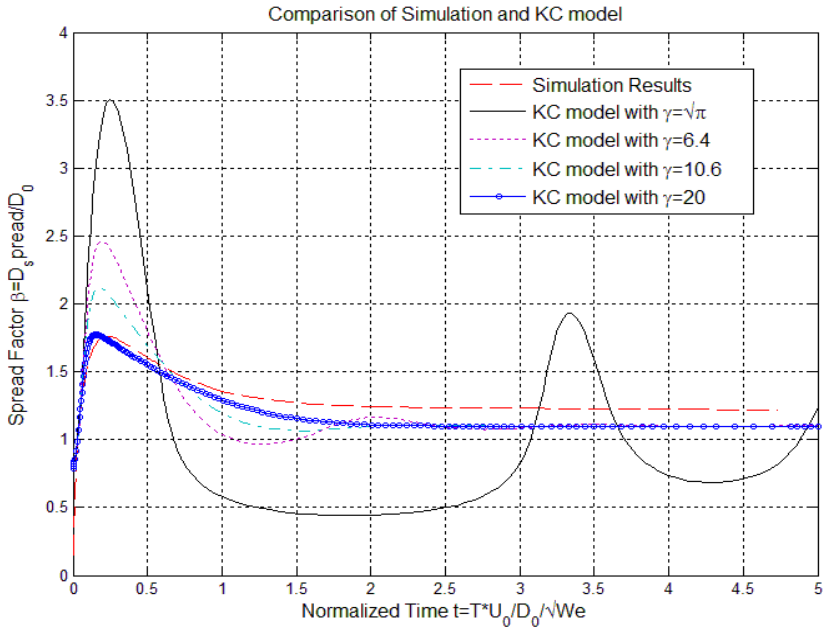

Figure 5 Comparison between simulation and KC model

Both BBT and KC models assume that the dissipation mainly occurs in the boundary layer. In contrast, Attane et al. [28] used a rimmed cylinder to approximate the shape of the droplet during spreading and further assumed that the rolling motion occurring in the rim promoted an additional dissipation mechanism. They proposed the AGM model:

$$\frac{1}{12}\frac{d}{dt}\left[\left(\frac{2}{3}+\frac{1}{45}\frac{1}{r^6}\right)\left(\frac{dr}{dt}\right)^2\right]+\frac{d}{dt}\left[r^2(1-cos\theta_e)+\frac{1}{3r}\right]+4Oh(3r^4+\frac{2}{3r^2}+sr)\left(\frac{dr}{dt}\right)^2 = 0 \quad (16)$$

with the initial conditions:

$$[r_0^2(1-cos\theta_e)+\frac{1}{3r_0}]_{for\ \theta_e<109^\circ} = 1; r_0 = 0.39\ for\ \theta_e > 109^\circ$$

$$\frac{dr}{dt}|_{t=0} = \sqrt{We}\left(\frac{2}{3}+\frac{1}{45}\frac{1}{r^6}\right)^{-1/2}$$

where $r = \frac{R}{D_0}$; $s = 1.41Oh^{-2/3}$ and the coefficient 1.41 in the parameter s is adjustable. The comparison is shown in Figure 6, which indicates that when the coefficient-multiplier goes to 0.45, the early stage of the spreading agrees well, and the long-term spreading dynamics predictions agree well between each other when s takes its default value.

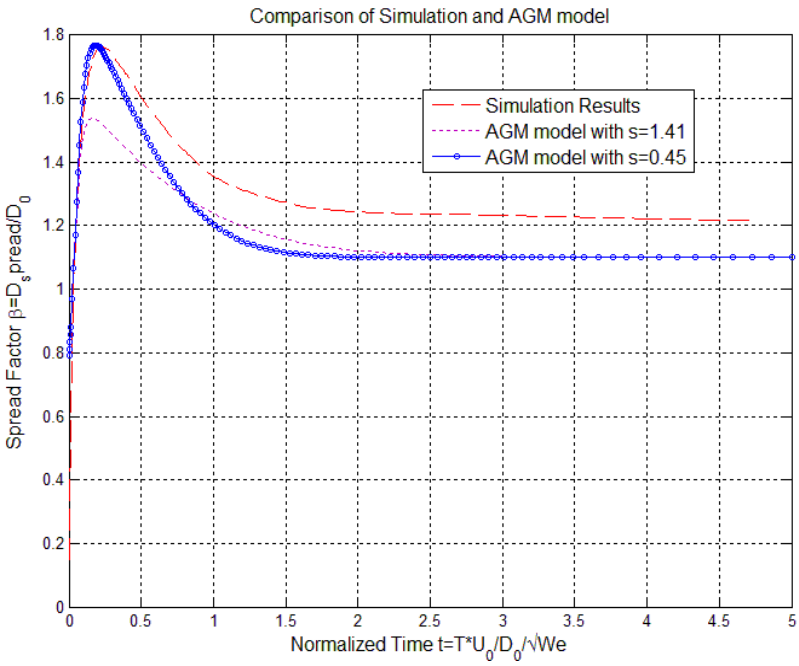

Figure 6 Comparison between simulation and AGM model

5. Experimental validation

To further validate the numerical model, experimental validation is necessary. Although there is a large body of experimental results in literature, few of them focus on the droplet size at the micron scale due to the difficulty of observation. In order to obtain similar droplet impact behavior with our interests, an experiment with a Weber number of interest was chosen for comparison. A water drop impact on a steel substrate with Weber number of 27 and contact angle of $\pi/2$ [31] is selected to compare with the simulation results, as shown in Figure 7, which is quite excellent during the early stage of the spreading (left panel).

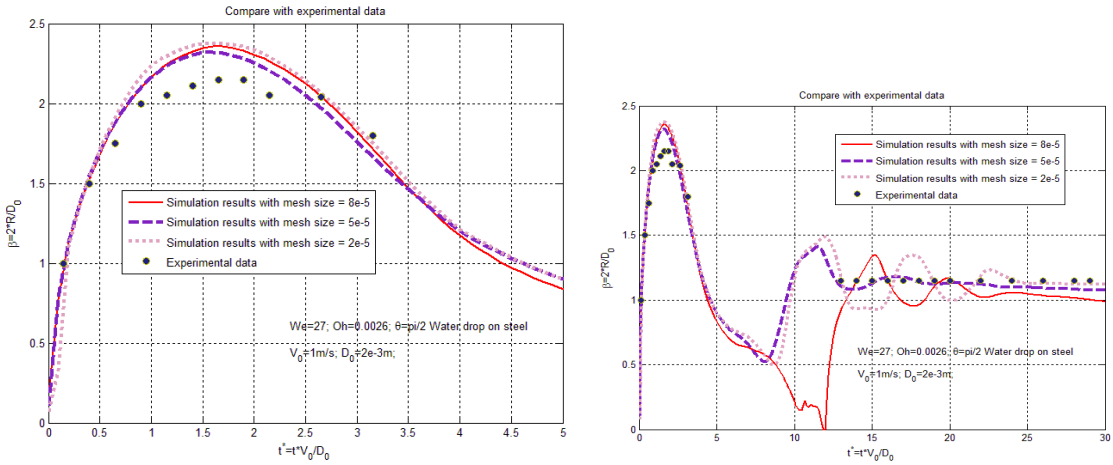

Figure 7 Comparison between experimental data and simulation: early stage(left); all time (right)

6. Impact of Polyurethane droplet

A thermoplastic polyurethane material is of particular interest in this paper due to its potential SFF applications. The fluid properties of polyurethane are taken from [36] as shown in Table 3.

Table 3 Impact conditions and fluid properties of polyurethane

	Droplet Radius	Contact Angle	Impact Velocity	Dynamic Viscosity	Surface Tension	Droplet Density
Value	25μm	$\pi/2$	10 m/s	3 Pa·s	0.029 N/m	1050 kg/m^3

Using the simulation conditions from Table 3, simulation results are shown in Figure 8. The time scale of spreading is increased, as compared to water, to about 0.1 second due to the higher viscosity of polyurethane and the maximum radius of the wetted area is only slightly larger than the equilibrium radius with no oscillation. As such, droplet impact behavior for high viscosity fluids is simpler than for low viscosity fluids, indicating that manufacturing process control may be simpler than in current printing processes.

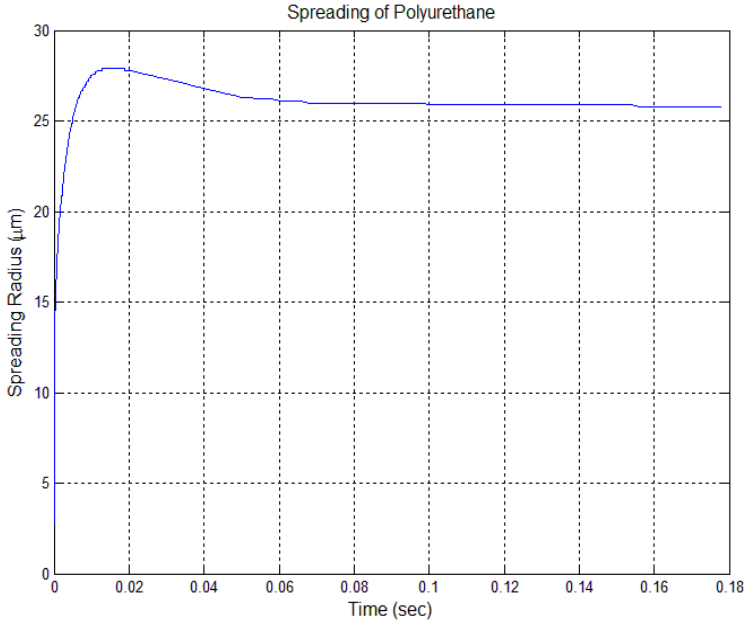

Figure 8 Simulation result of the spreading of polyurethane droplet

The BBT model and KC model are fundamentally unable to predict the spreading of the fluid at such high viscosity because they do not incorporate all the physics of viscous dissipation, as in the AGM model. Simulation results are compared with that of the AGM model as shown in Figure 9. The AGM model predictions compare well with simulations on the time scale for droplet spreading before reaching an equilibrium state. However, there are qualitative differences in dynamics of the droplet behavior (e.g., the AGM model does not predict a droplet recoil), as well as the quantitative discrepancy in the maximum and final spreading radii. Yes, the AGM model may be sufficiently accurate to make quick estimations for the process design, while using detailed and computationally intensive simulations for process refinement and optimization.

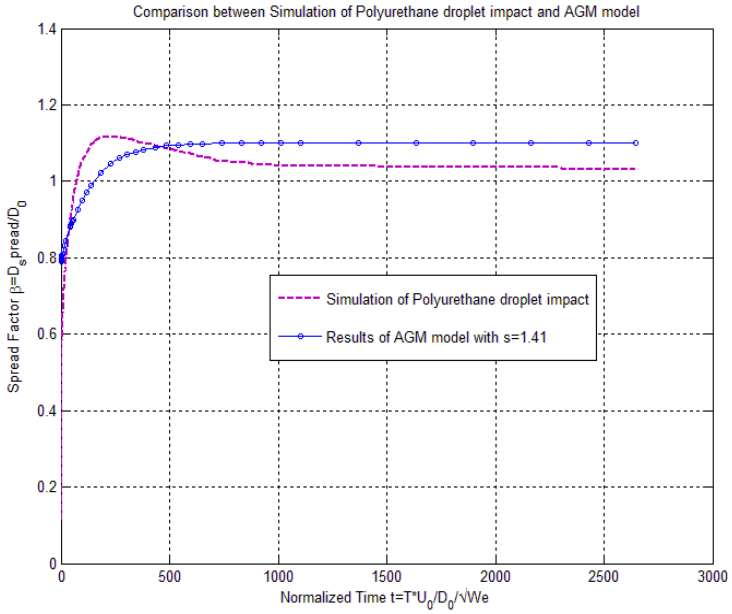

Figure 9 Comparison between simulation and AGM model

7. Conclusion

Previous research on droplet impact and hardening has been reviewed for SFF using ink-jet printing methods. A numerical model has been developed to simulate the transient fluid dynamics during droplet impact and spreading using phase-field method within an Eulerian fixed grid. A typical case under impact conditions of interest is presented to illustrate the implementation of the numerical simulation. Then two critical parameters for manufacturing, namely the equilibrium and maximum spreading radii, are calculated using both validated empirical analytical models and our numerical model and the comparison shows that the results agree very well. Further, three well known 1-D models are then used to calculate the dynamic spreading process which is compared with the spreading process computed by the proposed numerical model. By tuning the adjustable parameters of the analytical models, good agreements between the simulations and analytical results has been demonstrated. Complimentary to analytical validation of the numerical model, experimental data from literature was successfully used to validate the numerical model under relevant impact conditions. Finally, the impact of polyurethane droplet that is of particular interest for potential SFF applications is simulated using the proposed numerical model and compared with those three 1-D models. Results illustrate that the detailed understanding of the spreading process, as enabled by the CFD simulations, is essential to predict droplet behavior for ink-jet printing of complex engineering materials. Further, results show that only one of the simplified 1-D models (the AGM model) is able to predict the impact behavior of high viscosity fluids due to its incorporation, albeit rather simplistic, of viscous dissipation.

Acknowledgement

We gratefully acknowledge the U.S. National Science Foundation, through award DMI-0900322. Any opinions, findings, and conclusions or recommendations expressed in this publication are those of the authors and do not necessarily reflect the views of the National Science Foundation.

References

[1] A. L. Yarin, "Drop impact dynamics: Splashing, spreading, receding, bouncing," *Ann. Rev. Fluid Mech,* vol. 38, pp. 159-192, 2006.

[2] K. Mramor, "No Splash on the Moon," University of Ljubljana2007.

[3] S. L. Horstmeyer, "Deformation of water drops in the air," in *http://www.shorstmeyer.com/wxfaqs/float/dropdeform.html*, ed, 2008.

[4] E. B. Dussan, "On the spreading of liquids on solid surfaces: static and dynamic contact lines," *Annual Review of Fluid Mechanics,* vol. 11, pp. 371-400, 1979.

[5] N. Nagai, and V.P. Carey, "Assessment of surface wettability and its relation to boiling phenomena," in *Proceedings of the 2001 ASME International Mechanical Engineering Congress and Exposition*, New York, NY. USA, 2001.

[6] V. P. Carey, "Liquid-vapor phase change phenomena, an introduction of vaporization and condensation processes in heat transfer equipment," *Taylor and Francis, Series in Chemical and Mechanical Engineering,* 1992.

[7] R. Rioboo, M. Marengo, and C. Tropea, "Time evolution of liquid drop impact onto solid, dry surfaces," *Experiments in Fluids,* vol. 33, pp. 112-124, 2002.

[8] S. Schiaffino, and A.A. Sonin, "Molten droplet deposition and solidification at low Weber numbers," *Phys. Fluids,* vol. 9, pp. 3172-3187, 1997.

[9] A. M. Worthington, "On the forms assumed by drops of liquids falling vertically on a horizontal plate," *Proc. R. Soc. London,* vol. 25, pp. 261-271, 1876.

[10] L. Xu, W.W. Zhang and S.R. Nagel, "Drop splashing on a dry smooth surface," *Phys. Rev. Lett.,* vol. 94, p. 184505, 2005.

[11] Lei Xu, L. Barcos, and S.R. Nagel, "Splashing of liquids: Interplay of surface roughness with surrounding gas," *PHYSICAL REVIEW E,* vol. 76, p. 066311, 2007.

[12] R.E. Pepper, L. Courbin and H.A Stone, "Splashing on elastic membranes: the importance of early-time dynamics," *Phys. Fluids,* vol. 20, p. 082103, 2008.

[13] G. Astarita, "Dimensional analysis, scaling, and orders of magnitude," *Chemical Engineering Science,* vol. 52, pp. 4681-4698, 1997.

[14] G. McHale, S. M. Rowan, and M. I. Newton, "Frenkel's method and the spreading of small sperical droplets," *J. Phys. D,* vol. 27, p. 2619, 1994.

[15] Z. Zhao, D. Poulikakos and J. Fukai, "Heat transfer and fluid dynamics during the collision of a liquid droplet on a substrate - I. Modeling," *International Journal of Heat and Mass Transfer,* vol. 39, pp. 2771-2789, 1996.

[16] M. Sussman, P. Smereka, and S. Osher, "A level set approach for computing solutions to incompressible two-phase flow," *J. Comp. Phys.,* vol. 114, pp. 146-159, 1994.

[17] F.H. Harlow, and J.E. Welch, "Numerical calculation of time dependent viscous incompressible flow of fluid with free surface," *Physics of Fluids,* vol. 8, pp. 2182-2189, 1965.

[18] M. Bussmann, J. Mostaghimi and S. Chandra, "On a three-dimensional volume tracking model of droplet impact," *Physics of Fluids,* vol. 11, pp. 1406-1417, 1999.

[19] P. Yue, C. Zhou, J.J. Feng, C.F. Olliver-Gooch, and H.H. Hu, "Phase-field simulations of interfacial dyanmics in viscoelastic fluids using finite elements with adaptive meshing," *J. Comp. Phys.,* vol. 219, pp. 47-67, 2006.

[20] B. Kang, Z. Zhao and D. PouLikakos, "Solidification of liquid metal droplets impacting sequentially on a solid surface," *ASME Journal of Heat Transfer,* vol. 116, pp. 436-445, 1994.
[21] M. Francois, "Computations of drop dynamics with heat transfer," PhD, University of Florida, 2002.
[22] O. Aydin, and W.J. Yang, "On microtransport phenomena in minute droplets: a critical review," *Applied Mechanics Review,* vol. 53, pp. 101-116, 2000.
[23] A.M. Trommelen, and E.J. Crosby, "Evaporation and drying of drops in superheated vapor," *American Institute of Chemical Engineers Journal,* vol. 16, pp. 857-866, 1970.
[24] D.H. Charlesworth, and W.R. Marshall, "Evaporation from drops containing dissolved solids," *American Institute of Chemical Engineers Journal,* vol. 6, pp. 9-23, 1960.
[25] C. N. B. Alec B. Scranton, Robert W. Peiffer, Ed., *Photopolymerization: Fundamentals and Applications*. An American Chemical Society Publication, 1997, p.^pp. Pages.
[26] I. Gibson, D.W. Rosen, and B. Stucker, *Additive Manufacturing Technologies: Rapid Prototyping to Direct Digital Manufacturing*: Springer, 2009.
[27] F.H. Harlow, and J.P. Shannon "The splash of a liquid drop," *Journal of Applied Physics,* vol. 38, pp. 3855-3866, 1967.
[28] P. Attané, F. Girard and V. Morin, "An energy balance approach of the dynamics of drop impact on a solid surface," *Physics of Fluids,* vol. 19, p. 012101, 2007.
[29] B.L. Scheller, and D.W. Bousfield, "Newtonian drop impact with a solid surface," *AIChE J. ,* vol. 41, p. 1357, 1995.
[30] A. Asai, M. Shioya, S. Hirasawa, and T. Okazaki, "Impact of an ink drop on paper," *J. Imaging Sci. Technol.,* vol. 37, p. 205, 1993.
[31] M. Pasandideh-Fard, Y. M. Qiao, S. Chandra, and J. Mostaghimi, "Capillary effects during droplet impact on a solid surface," *Phys. Fluids,* vol. 8, p. 1344, 1996.
[32] S. Chandra, and C.T. Avedisian, "On the collision of a droplet with a solid surface," in *Proceedings of the Royal Society, Series A*, London, 1991, pp. 13-41.
[33] T. Mao, D. C. S. Kuhn, and H. Tran, "Spread and rebound of liquid droplets upon impact on flat surfaces," *AIChE J.,* vol. 43, p. 2169, 1997.
[34] S. E. Bechtel, D. B. Bogy, and F. E. Talke, "Impact of a liquid drop against a flat surface," *IBM J. Res. Dev.,* vol. 25, p. 963, 1981.
[35] H.-Y. Kim, and J.-H. Chun, "The recoiling of liquid droplets upon collision with solid surface," *Physics of Fluids,* vol. 13, pp. 643-659, 2001.
[36] J.M. Meacham, A. O'Rourke, Y. Yang, A.G. Fedorov, F.L. Degertekin, and D.W. Rosen, "Micromachined Ultrasonic Print-Head for Deposition of High-Viscosity Materials," *Journal of Manufacturing Science and Engineering,* vol. 132, p. 030905, 2010.